Reconstructing the oxygen depth profile in the Arabian Sea during the last glacial period

Wanyi Lu [1]*, Kassandra M. Costa [1], Delia W. Oppo [1]

1 Department of Geology and Geophysics, Woods Hole Oceanographic Institution, Woods Hole MA, USA

*Correspondence to wlu@whoi.edu

Abstract

Reconstructing the strength and depth boundary of oxygen minimum zones (OMZs) in the glacial ocean advances our understanding of how OMZs respond to climate changes. While many efforts have inferred better oxygenation of the glacial Arabian Sea OMZ from qualitative indices, oxygenation and vertical extent of the glacial OMZ is not well quantified. Here we present glacial-Holocene oxygen reconstructions in a depth transect of Arabian Sea cores ranging from 600 to 3,650 m water depths. We estimate glacial oxygen concentrations using benthic foraminiferal surface porosity and benthic carbon isotope gradient reconstructions. Compared to the modern Arabian Sea, glacial oxygen concentrations were approximately 10–15 µmol/kg higher in the shallow OMZ (<1,000 m), and 5–80 µmol/kg lower at greater depths (1,500–3,650 m). Our results suggest that the OMZ in the glacial Arabian Sea was slightly better oxygenated but remained in the upper 1,000 m. We propose that the small increase in oxygenation of the Arabian Sea OMZ during the last glacial period was due to weaker upper ocean stratification induced by stronger winter monsoon winds coupled with an increase in oxygen solubility due to lower temperatures, counteracting the effects of more oxygen consumption resulting from higher primary productivity. Large-scale changes in ocean circulation may have also contributed to better ventilation of the glacial Arabian Sea OMZ.

Key Points

1. The glacial Arabian Sea OMZ was slightly weaker but spanned the same depth as modern.
2. Enhanced oxygen supply locally and/or from the south likely explained the weaker OMZ in the glacial Arabian Sea.
3. Bottom water oxygen in the deep glacial Arabian Sea ranged between 50 and 100 µmol/kg.

1. Introduction

Dissolved oxygen in the global oceans has been declining since the 1960s due to lower oxygen solubility related to ocean warming and increased oxygen consumption related to more nutrient input (Breitburg et al., 2018; Schmidtko et al., 2017). Oxygen Minimum Zones (OMZs) are important oceanic regions because of their unique low-oxygen ecosystems where many organisms live, and also because of their important roles in global marine carbon and nitrogen cycles. Any future changes in the OMZ volumes could have large impacts on marine and estuarine fisheries and ecosystem (Breitburg et al., 2018). However, climate model simulations fail to reproduce historical oxygen data (Bopp et al., 2013) and it is uncertain how much and when the OMZ volumes will change under global warming scenarios (Bopp et al., 2013; Fu et al., 2018). Models are also unable to tease apart the subtle balance among temperature-related oxygen solubility, ventilation, and biological effects on the OMZs and between regions (Resplandy, 2018). Paleo-oxygen reconstructions of the last glacial period (LGP, here broadly defined as 18,000–32,000 years ago, or 18–32 ka) provide valuable targets for comparing with, and potentially validating, climate models. Insights on how and why the OMZs changed in the past may help improve future projections.

The Arabian Sea, Eastern Tropical North Pacific (ETNP), and Eastern Tropical South Pacific (ETSP) are the three major OMZs and thus important regions to understand how oxygen responded to climate changes in the past. Compilations of qualitative paleo-oxygen reconstructions from the global ocean have suggested a generally better-oxygenated upper ocean but less-oxygenated deep ocean during the Last Glacial Maximum compared to modern/Holocene (Jaccard & Galbraith, 2012; Moffitt et al., 2015). Recent studies have used semi-quantitative bottom water oxygen (BWO) proxies to provide constraints on past BWO. These include benthic foraminiferal assemblages (Erdem et al., 2020; Tetard et al., 2021) and morphology (Glock et al., 2022; Rathburn et al., 2018), benthic carbon isotope gradients (Δδ13C) (Hoogakker et al., 2015; McCorkle & Emerson, 1988), benthic I/Ca (Glock et al., 2014; Lu et al., 2020), C37 alkenone preservation in the sediments (Anderson et al., 2019), and bulk sediment U/Ba (Costa et al., 2023). The sensitivity, uncertainty, and limitations of each semi-quantitative BWO proxy are summarized in Lu et al. (2022). With the exception of Δδ13C and U/Ba, these proxies are only sensitive to low BWO conditions (<50 or <100 μmol/kg), and have been mostly applied and tested at sites from the Pacific and Atlantic oceans. Previous studies have suggested weaker OMZ in the upper ocean and less-ventilated deep water in the Arabian Sea during the LGP compared to modern (Altabet et al., 2002; Gaye et al., 2018; Pichevin et al., 2007; Reichart et al., 1998; Schmiedl & Leuschner, 2005; Schmiedl & Mackensen, 2006; Sirocko et al., 2000), but as yet there is no quantitative assessment of the magnitude of oxygen changes in the Arabian Sea during the LGP.

In this study, we use two independent, semi-quantitative BWO proxies – benthic foraminiferal surface porosity (i.e., surface area percentages covered by pores) and $\Delta\delta^{13}C$ – to reconstruct the glacial oxygen profile in the Arabian Sea. Below BWO concentrations of 100 µmol/kg, the benthic surface porosity of *Cibicidoides* spp. shows a strong negative logarithmic correlation with BWO, both globally and regionally in the Arabian Sea (Lu et al., 2022; Rathburn et al., 2018). The proxy is based on the theory that in low-oxygen environments, benthic foraminifera require more and/or larger pores (i.e., higher porosity) on the surface to facilitate gas exchange, while in oxic conditions, foraminifera rely mainly on their aperture (the primary opening on the test) for respiration. Furthermore, surface porosity seems to be independent from other pore functions such as taking up organic carbon for food and releasing respiratory CO_2; thus BWO seems to be the potential dominant control on surface porosity (Lu et al., 2022).

The $\Delta\delta^{13}C$ proxy is calculated as the $\delta^{13}C$ difference between bottom water (as recorded by the epifaunal foraminifera *Cibicidoides wuellerstorfi*) and anoxic pore water (as recorded by the deep infaunal foraminifera *Globobulimina* spp.) (Hoogakker et al., 2015; McCorkle & Emerson, 1988). The proxy is based on the assumption that higher BWO leads to more organic matter remineralization, which releases relatively low $\delta^{13}C$ carbon into the pore water, thus increasing the $\delta^{13}C$ gradient between bottom water and anoxic pore water. However, the $\delta^{13}C$ in pore water can be lowered by denitrification mechanisms by *Globobulimina* spp. and sulfate reduction processes (Jacobel et al., 2020; McCorkle & Emerson, 1988). Thus the Δδ13C-based BWO values are likely maximum estimates (Jacobel et al., 2020), and can be considerably higher than those estimated from other independent proxies in some regions (Costa et al., 2023).

Given the uncertainty and limitations of each paleo-BWO proxy, we use a multi-proxy approach to provide robust paleo-BWO estimates in the glacial Arabian Sea. We compare the benthic surface porosity and $\Delta\delta^{13}C$ proxies to further evaluate their applicability and limitations, and compare them with published qualitative paleo-oxygen records. Lastly, we compare the glacial oxygen depth profiles from the Arabian Sea and the ETSP off the Peruvian Margin (Erdem et al., 2020; Glock et al., 2022; Scholz et al., 2014), and we explore the driving mechanisms of oxygen changes in these two regions.

2. Materials and Methods

2.1. Study areas and modern context of OMZs

In the modern Arabian Sea, the OMZ (here broadly defined as O_2 < 20 µmol/kg) occurs between 200 and 1200 m, where North Indian Intermediate Water (NIIW) is the dominant water mass, itself a mixture of aged Antarctic Intermediate Water (AAIW), Subantarctic Mode Water, and Indonesian Intermediate Water, advected from the south through the Somali current (Fig. 1) (Morrison et al., 1999; Olson et al., 1993). Denitrification, where nitrate is reduced to nitrite, generally occurs in the 200 - 800 m depth range of the OMZs, where O_2 is < 10 µmol/kg (Morrison et al., 1999; Naqvi, 1987). In the Arabian Sea, this depth range is also influenced by 1) Persian Gulf Water (PGW) entering from the north near ~ 300 m depths, with source oxygen concentrations of ~110 µmol/kg; and 2) Red Sea Water (RSW) entering from west sinking to depths between 600 and 1000 m, with source oxygen concentrations of ~150 µmol/kg (Olson et al., 1993). The perennial OMZ in modern Arabian Sea is caused by a combination of relatively low-oxygen initial water, and high oxygen consumption due to high organic matter input during the Indian summer and winter monsoons (Olson et al., 1993). Below the OMZ center, the deep water masses between 1500 m and 3800 m are dominated by North Indian Deep Water (NIDW) with source oxygen concentration of ~90 - 150 µmol/kg, which originated from aged North Atlantic and Circumpolar Deep Water (NADW and CDW) (You, 2000).

The size and intensity of Arabian Sea OMZs are thought to be sensitive to changes in Indian monsoons both on decadal (Lachkar et al., 2018) and millennial timescales (Reichart et al., 1998; Schmiedl & Leuschner, 2005; Schmiedl & Mackensen, 2006). During the summer monsoon seasons, southwesterly winds drive strong upwelling off Somalia and Oman, bringing cold and nutrient-rich water to the surface and sustaining high productivity (Lachkar et al., 2018; Nair et al., 1989). During the winter monsoon seasons, dry cold northeasterly winds from the Asian continent lower the sea surface temperature (SST) and increase the depth of convective mixing, bringing cold and nutrient-rich subsurface water to the euphotic zone (Lachkar et al., 2018; Nair et al., 1989). Past changes in monsoon intensity can therefore influence oxygen consumption through biological productivity changes.

2.2. Samples

A total of six core sites of Arabian Sea were selected to form a depth transect with water depths ranging from 600 to 3650 m (Fig. 1 and Table 1). We combined our new records with two published semi-quantitative paleo-BWO records (TN041-8PG/JPC, water depth 761 m (Lu et al.,

2022) and GeoB3004 (1803 m, (Schmiedl & Mackensen, 2006)). Four RC27 cores were sampled from the Lamont-Doherty Core Repository, and two TN041/047 cores were sampled from the Woods Hole Oceanographic Institution (WHOI) Seafloor Samples Repository.

All samples were first freeze-dried, then wet-sieved to > 63 µm fraction with de-ionized water, and oven-dried at 45°C. Benthic foraminifera *Cibicidoides* spp. and *Globobulimina affinis* were picked from the > 212 µm fraction. In three cores within the OMZ (RC27-14, TN041-8PG/JPC, and RC27-23, water depths 596 – 820 m), the dominant species is an unidentified *Cibicioides* spp. with sparse occurrences of *Planulina* sp. and *C. wuellerstorfi*. In core TN041-2PG (depth 1428 m), both *C. wuellerstorfi* and *C. pachyderma* are abundant. The *Cibicidoides* spp. in cores of RC27-61 (1890 m) and RC27-42 (2020 m) include *C. wuellerstorfi*, *C. pachyderma*, and *C. lobatulus*, with *C. lobatulus* being the dominant species. In the deepest core (TN047-6GGC, 3652 m), *C. wuellerstorfi* is the dominant species. Planktic foraminifera *Globigerinoides ruber* in core TN041-2PG were picked from > 250 µm fraction for isotope stratigraphy and radiocarbon dating.

2.3. Age models

The age models for four RC27 cores were produced by linear interpolation between previously published ages. RC27-14 and RC27-23 were based on correlation between bulk sediment $\delta^{15}N$ and Greenland ice core $\delta^{18}O$ (Altabet et al., 2002). RC27-61 was based on correlation between planktic $\delta^{18}O$ and global stacked $\delta^{18}O$ records (Clemens & Prell, 1990). RC27-42 was based on planktic $\delta^{18}O$ stratigraphy and six radiocarbon dates (Pourmand et al., 2007).

A new age model was created for core TN041-2PG. Ages for core TN041-2PG were first estimated using *G. ruber* $\delta^{18}O$ stratigraphy, then two samples, one from the core top and one from near the core bottom, were selected for radiocarbon dating. Each radiocarbon date represents an average of around 300 individuals of *G. ruber*. Both accelerator mass spectrometry (AMS) ^{14}C dates were acquired at the National Ocean Sciences Accelerator Mass Spectrometry facility at WHOI. Both radiocarbon dates were calibrated against Marine20 using Calib8.20 (Stuiver et al., 2022) using an Arabian Sea regional marine radiocarbon reservoir age correction $\Delta R = 93\pm61$ years (Table 2) (Heaton et al., 2020). The age model was then constructed using the BACON v2.3.91 package in R (Blaauw & Christeny, 2011). We also updated the age models for TN047-6GGC which has six radiocarbon ages (Dahl & Oppo, 2006) with Marine20 and BACON package. The *G.*

ruber $\delta^{18}O$ record of TN041-2PG was similar to those from two nearby cores, TN041-8PG/JPC (Lu et al., 2022) and RC27-42 (Pourmand et al., 2007) (Fig. S1).

2.4. Benthic foraminiferal surface porosity

We measured the surface porosity of *Cibicidoides* spp. following (Petersen et al., 2016). Around 1-16 specimens in each sample were analyzed, for a total of 790 individuals reported in this study. We scanned 68 individuals in core RC27-14; 83 individuals in core RC27-23; 140 individuals in core TN041-2PG; 239 individuals in core RC27-61; 96 individuals in core RC27-42; and 164 individuals in core TN047-6GGC. Because no systematic surface porosity offsets were found among different *Cibicidoides* spp. in the same sample in the core-top calibration (Lu et al., 2022; Rathburn et al., 2018), we reported the average and standard deviation of porosity of all *Cibicidoides* spp. in each sample.

Photos were taken using a Scanning Electron Microscope (SEM) (Hitachi model TM3000) at WHOI. The dorsal side of each specimen (side that is exposed to bottom water) was imaged. ImageJ, a semi-automatic image-processing software (available at https://imagej.nih.gov/ij/), was then used to calculate the surface porosity, based on a grayscale threshold applied to a specific frame. Because the last chamber is often broken or absent, porosity was calculated for the penultimate chamber of all specimens, which represents the same ontogenetic stage (Petersen et al., 2016; Rathburn et al., 2018). The frame was placed in an area representative of the whole chamber, usually the inner, flat portion of the chamber, to avoid including distorted pores. Frames were manually positioned using a macro developed by (Petersen et al., 2016), which allowed us to place a frame of the same size on all SEM images. Selected representative SEM photos of *Cibicidoides* spp. are shown in Fig. 2.

2.5. Stable isotopes

Carbon and oxygen isotopic analyses were made using a Finnigan MAT253 mass spectrometer at WHOI with a long-term laboratory precision (1σ) of the NBS-19 carbonate standard of ± 0.07 ‰ for $\delta^{18}O$ and ± 0.03 ‰ for $\delta^{13}C$. The isotopes on *Cibicidoides* spp. were performed after benthic surface porosity analyses were completed. Each isotope analysis used 3 – 4 specimens of *G. ruber*, 1 – 2 specimens of *Cibicidoides* spp., and 1 – 2 specimens of *G. affinis*.

Because the $\Delta\delta^{13}C$-based BWO values were found to be much higher than those estimated from surface porosity, benthic I/Ca, authigenic uranium proxies in site TN041-8PG/JPC within the OMZ center (Lu et al., 2022), we did not make additional measurements of $\Delta\delta^{13}C$ in cores RC27-14 and RC27-23. We report new $\Delta\delta^{13}C$ records in cores RC27-61, RC27-42 and TN047-6GGC.

3. Results

3.1. Benthic surface porosity-based BWO records

For the two new records from within the OMZ (RC27-14 and RC27-23), the benthic surface porosity values are high (10 - 40%) throughout, consistent with those found previously in core TN041-8PG/JPC (Fig. 3) (Lu et al., 2022). In core RC27-14 (596 m), surface porosity values are ~15% in the LGP, increase to ~ 25% between 18 and 12 ka, with limited benthic specimens found in Holocene sediment. In core RC27-23 (820 m), surface porosity is relatively lower in the LGP and deglaciation (23 - 12 ka, average 21 ± 2 %, n = 8) compared to those in late Holocene ages (7 - 0 ka, average 30 ± 4 %, n = 5). In core TN041-2PG (1428 m), surface porosity values show small variations, falling between 10 and 15% throughout the core. In the three deeper cores below the OMZ (RC27-61, RC27-42, and TN047-6GGC, depths between 1.9 and 3.7 km), surface porosity in most samples is < 10%.

The surface porosity-based BWO equation is only applicable when BWO < 100 μmol/kg (Lu et al., 2022). Six sites (all except for TN047-6GGC) have modern BWO < 100 μmol/kg, and because redox-sensitive trace element records suggest lower glacial BWO in deep Arabian Sea (Sirocko et al., 2000), we converted the surface porosity values in these six cores into BWO using the Arabian Sea regional calibration equation (Lu et al., 2022). We did not apply the calculation on core TN047-6GGC because modern BWO at this site is ~130 μmol/kg and exceeds the calibration limit of the proxy. As a result, glacial BWO may range between 0 and 130 μmol/kg. The surface porosity-based BWO uncertainties were previously estimated to be ±10 μmol/kg at 20 μmol/kg (with average porosity S.D. of 8%) and to increase to ±33 μmol/kg at 80 μmol/kg (with average porosity S.D. of 2%).

In three shallower cores (< 820 m), the glacial BWO was around 20 μmol/kg, implying slightly better oxygenation than modern. In the deeper cores (1400-2000 m), porosity-based BWO values for the LGP are generally comparable to the modern value, with ~20 μmol/kg fluctuations for TN041-2PG, and 30 - 40 μmol/kg fluctuations for both RC27-61 and RC27-42. In core TN047-

6GGC (3700 m), we infer glacial BWO ranging between 50 and 130 μmol/kg based on low benthic surface porosity and redox-sensitive trace element records (Sirocko et al., 2000).

3.2. Benthic $\Delta\delta^{13}C$-based BWO records

As expected, the $\delta^{18}O$ glacial values of both *C. wuellerstorfi* and *G. affinis* in cores RC27-61, RC27-42, and TN047-6GGC are higher than Holocene values, reflecting changes in both temperature and seawater $\delta^{18}O$ (Fig. 4). In cores GeoB3004 and RC27-61 (1800-1900 m), $\delta^{13}C$ in both *C. wuellerstorfi* and *G. affinis* are comparable during the Holocene and the LGP. In core RC27-42 (2000 m), $\delta^{13}C$ in *C. wuellerstorfi* is ~0.2 ‰ lower in LGP samples compared to Holocene samples; $\delta^{13}C$ in *G. affinis* in the LGP are around -1.0 ‰, similar to the Holocene. In core TN047-6GGC (3700 m), $\delta^{13}C$ values in *C. wuellerstorfi* are ~0.5 ‰ lower in LGP samples compared to Holocene samples; $\delta^{13}C$ in *G. affinis* ranges between -1.5 and -2 ‰ throughout the core, with no clear down-core trend.

For the four cores deeper than 1800 m, we converted the $\Delta\delta^{13}C$ values into BWO using the global calibration equation, with uncertainties estimated to be ±17 μmol/kg (Hoogakker et al., 2015). The updated $\Delta\delta^{13}C$-based BWO values in core GeoB3004 (1800 m) (Schmiedl & Mackensen, 2006) are highly variable in the last 32 ka, fluctuating between 30 and 120 μmol/kg (Fig. 4C). In core RC27-61 (1900 m), three samples show $\Delta\delta^{13}C$-based BWO within 20-30 μmol/kg of the modern value. In core RC27-42 (2000 m), the $\Delta\delta^{13}C$-based BWO in three LGP samples are 15-30 μmol/kg lower than the modern value, while one Holocene sample has $\Delta\delta^{13}C$-based BWO ~20 μmol/kg higher than the modern value. In core TN047-6GGC (3700 m), the $\Delta\delta^{13}C$-based BWO values are ~100 μmol/kg during the LGP, generally increase during the deglaciation and Holocene, and reach ~225 μmol/kg at 2.5 ka. In three samples close to the core top (sample depths < 10 cm), two values suggest $\Delta\delta^{13}C$-based BWO close to the modern value, and one suggests ~60 μmol/kg higher than the modern value.

4. Discussion

4.1. BWO proxy intercomparison

The two new benthic surface porosity records from RC27-14 (596 m) and RC27-23 (820 m) from the OMZ center are consistent with the published record from TN041-8PG/JPC (761 m) (Lu et al., 2022). All three sites indicate that the OMZ was weaker during the LGP than modern, consistent with qualitative paleo-redox records, such as bulk sedimentary $\delta^{15}N$ (Altabet et al., 2002; Gaye et al., 2018; Pichevin et al., 2007; Reichart et al., 1998). Our estimates constrain the glacial OMZ to be only slightly better oxygenated, by about 10 - 15 µmol/kg. In RC27-61 (1890 m) and RC27-42 (2020 m), both benthic surface porosity and $\Delta\delta^{13}C$ reconstructions suggest glacial BWO fluctuating within 20 - 30 µmol/kg of modern BWO. At water depths between ~1500 and ~2000 m, BWO was not substantially different between the LGP and modern (Fig. 5A).

In core TN047-6GGC (depth 3652 m), the overall low benthic surface porosity < 10% and published redox-sensitive trace element records from nearby sites (Sirocko et al., 2000) suggest glacial BWO ranging between 50 and 130 µmol/kg in the deep Arabian Sea. The $\Delta\delta^{13}C$ record adds additional constraints, suggesting a maximum glacial BWO value of ~100 µmol/kg. In general, these independent BWO proxy reconstructions (benthic surface porosity, $\Delta\delta^{13}C$, and redox-sensitive trace elements) are consistent with each other, confirming that the glacial deep Arabian Sea was less oxygenated than modern. It has been suggested that $\delta^{13}C$ in *G. affinis* might be impacted by denitrification mechanisms, and sulfate reduction within the sediments which could reduce the $\delta^{13}C$ in the pore water where *G. affinis* calcify (Jacobel et al., 2020; McCorkle & Emerson, 1988), implying that $\Delta\delta^{13}C$ provides maximum estimates of BWO. Comparing the three samples close to the core top, the $\delta^{13}C$ values in *C. wuellerstorfi* are comparable, but one sample has relatively lower $\delta^{13}C_{G.\ affinis}$ (-2 ‰ vs. -1.5 ‰ in other two samples), resulting in its $\Delta\delta^{13}C$-based BWO ~60 µmol/kg higher than the modern value. Similar order of magnitude $\Delta\delta^{13}C$-based BWO offset are also found in the western Equatorial Atlantic and Eastern Equatorial Pacific (Costa et al., 2023). Thus, we assume the $\Delta\delta^{13}C$ record provides maximum BWO estimates.

In both RC27-61 (1890 m) and RC27-42 (2020 m), *C. wuellerstorfi* are scarce, so *C. pachyderma* and *C. lobatulus* were used for isotope analyses. The comparison of $\delta^{13}C$ of these three *Cibicidoides* species suggests that the downcore $\delta^{13}C$ offsets are highly variable among *C. wuellerstorfi*, *C. pachyderma*, and *C. lobatulus* (Fig. S2). This finding suggests that at least in the Arabian Sea, only *C. wuellerstorfi*, and not other *Cibicidoides* spp., should be used for $\Delta\delta^{13}C$-based BWO estimates.

4.2. Potential driving mechanisms of glacial OMZ in the Arabian Sea

Our new and published paleo-BWO records from eight sites ranging from 600-3700 m water depths provide the first semi-quantitative reconstruction of the glacial oxygen depth profile in the

Arabian Sea (Fig. 5A). Compared to modern, the glacial upper ocean OMZ was more oxygenated by 10 - 15 µmol/kg and the lower depth boundary of OMZ remained at ~1000 m; at 1500 m depth, oxygen concentrations were similar; and in the deep ocean (2000-3700 m), oxygen was lower by 5 - 80 µmol/kg, but the absolute concentrations remained between 50 - 100 µmol/kg.

As noted in Section 2.1, the modern Arabian Sea OMZ results from low oxygen supply by the mean ocean circulation combined with relatively high productivity fueled by the seasonal monsoons (Keeling et al., 2010; Olson et al., 1993). During the LGP, as a result of lower sea-level, the Persian Gulf dried out and the Red Sea outflow was reduced by ~85% (Rohling & Zachariasse, 1996), so these two relatively high-oxygen water masses did not ventilate the Arabian Sea OMZs. However, upper ocean oxygen increased, not decreased during the LGP, so the reduction of these flows to the Arabian Sea was not the major influence on the weaker OMZ. Indeed, model simulations suggest that the loss of the Persian Gulf source would have increased the suboxic volume below 200 m by 3%, with little impact on density structure and circulation (Lachkar et al., 2019). We thus explore two other options, a decrease in productivity and/or an increase of oxygen supply locally and/or from the south as drivers of the weaker OMZ in glacial Arabian Sea (Fig. 6).

A regional compilation of paleo-productivity reconstructions suggests generally higher productivity in the Arabian Sea during the LGP relative to Holocene (Zhou et al., 2022), which would have resulted in more oxygen consumption in the water column, reducing oxygen concentrations and strengthening the OMZ, rather than weakening it as we observe. We thus infer that there was a higher oxygen supply to the Arabian Sea OMZ during the LGP, compensating for the loss of the relatively minor high oxygen source waters from the Persian Gulf and Red Sea and more oxygen consumption due to higher productivity. Indeed, physical controls from temperature and ocean circulation changes have been proposed to explain reduced water column denitrification during the LGP (Galbraith et al., 2004; Meissner et al., 2005). More intense winter monsoon winds and/or an increase in its seasonal duration (Pourmand et al., 2007), coupled with 2 - 4°C colder SSTs (Dahl & Oppo, 2006; Pourmand et al., 2007), may have contributed to better oxygenation of the OMZ. While winter mixing in the modern Arabian Sea only extends to ~100 m depth, strengthened winter monsoon winds during the LGP might have resulted in convective mixing to as deep as ~800 m (Reichart et al., 1998), injecting oxygenated waters into the OMZ. In addition, both proxy records and model simulations suggest enhanced formation of AAIW, which may have reached northern Indian Ocean during the LGP (Galbraith et al., 2004; Pichevin et al., 2007; Schulte et al., 1999; Yu et al., 2018), and with higher oxygen concentrations (Muratli et al., 2010; Schulte et al., 1999), thus potentially providing higher oxygen supply from the south and help weaken the OMZ.

In summary, despite higher productivity and the associated greater oxygen consumption, the Arabian Sea OMZ was weaker in the LGP than in the Holocene. Consistent with previous studies, we suggest two potential mechanisms for the slightly higher oxygen levels in the upper ocean. First, a stronger winter monsoon may have resulted in deeper convective mixing, and coupled with colder glacial SSTs which increased oxygen solubility, injected relatively high oxygen surface waters into the OMZ. Second, enhanced formation of AAIW and with higher oxygen concentrations, also due to increased oxygen solubility, from the south may have contributed to more oxygen in the intermediate depths of Arabian Sea.

Lastly, in the deep Arabian Sea, the less-ventilated glacial conditions are likely to reflect ventilation changes in the source waters from Southern Ocean. Indeed, Nd isotope records suggest that less NADW but more AABW water reached the glacial Arabian Sea compared to the Holocene (Lathika et al., 2021; Piotrowski et al., 2009). The AABW/CDW water may have been less oxygenated during the LGP (Gottschalk et al., 2016, 2020), contributing to the deep-sea deoxygenation.

4.3. Comparing to the Peruvian Margin

We next compare the glacial OMZ profile of Arabian Sea to that of Peruvian Margin (Fig. 5B). The glacial oxygen profile from Peruvian Margin is based on a variety of semi-quantitative proxy records including benthic foraminifera assemblages (Erdem et al., 2020), benthic surface pore density (Glock et al., 2022), and redox-sensitive trace metals (Fe, Mo, and U) (Scholz et al., 2014). The glacial upper ocean (< 500 m) appears to have been slightly more oxygenated by ~5 - 10 μmol/kg compared to modern (Glock et al., 2022; Scholz et al., 2014), while data from sites at 1000-1200 m suggest similar BWO between LGP and modern (Erdem et al., 2020). Thus, the glacial OMZ changes seem to be similar in the Arabian Sea and Peruvian Margin, both having slightly higher oxygen concentrations and no changes in the depth of the OMZ lower boundary.

Similar physical control for the glacial upper ocean oxygenation has been proposed in Peruvian Margin: increased oxygen solubility related to ocean cooling and increased oxygen supply from source water (Galbraith et al., 2004; Glock et al., 2022; Meissner et al., 2005). On the other hand, glacial primary productivity in Peruvian Margin was suggested to be lower compared to modern (Glock et al., 2018), thus leading to less oxygen consumption in the upper ocean. This low glacial productivity on the Peru Margin compounded the gain of oxygen due cooling and the large-scale circulation In contrast, in the Arabian Sea, high productivity damped the oxygen increase due to cooling, enhance vertical mixing, and the large scale circulation. The shallow OMZ in the glacial Peruvian Margin seems to have decoupled from those from Eastern and Central Equatorial Pacific, which downward expansion of oxygen-depleted waters may have occurred during the LGP (Anderson et al., 2019; Hoogakker et al., 2018; Jacobel et al., 2020).

4.4. Implications for model-data comparison

As noted in the Introduction, improving the model performance/prediction to simulate the extent and timing of OMZ changes can benefit from reproducing paleo-oxygen records. Previous model simulations have mostly relied on qualitative paleo-oxygen records to validate the glacial simulation results, and proposed different driving mechanisms of glacial oxygenation changes (Bopp et al., 2017; Buchanan et al., 2016; Cliff et al., 2021; Galbraith & Jaccard, 2015; Schmittner & Somes, 2016; Somes et al., 2017; Yamamoto et al., 2019). The quantitative oxygen changes between the LGP and modern/Holocene vary among different models. For example, the simulated glacial oxygen in the upper North Indian Ocean ranges from ~20 to ~50 μmol/kg higher than modern. Our estimate of ~ 10-15 μmol/kg suggests that the lower range of these estimates is more likely. On the other hand, glacial simulations suggest that oxygen in deep North Indian Ocean ranged from ~10 to ~120 μmol/kg, with our results (Fig. 5) suggesting the lower range of these estimates is unlikely (Bopp et al., 2017; Schmittner & Somes, 2016; Somes et al., 2017; Yamamoto et al., 2019). Thus, although there is still relatively large uncertainty in oxygenation of the deep glacial Arabian Sea, the glacial oxygen depth profile reconstruction for Arabian Sea presented here is a valuable target for future model-data comparison, namely the 10 – 15 μmol/kg higher oxygen in upper ocean but with a similar OMZ depth boundary (at ~1000 m). Combined with model simulations, these constraints can help disentangle the relative contributions of temperature, ocean circulation, and biological effects on the OMZ changes.

5. Conclusions

We use the benthic surface porosity and $\Delta\delta^{13}C$ proxies to semi-quantitatively reconstruct the intensity and depth of the OMZ in the glacial Arabian Sea. The dual-proxy approach suggests a weaker OMZ but with a similar depth boundary as modern. In the deep Arabian Sea (~3700 m), the benthic surface porosity and $\Delta\delta^{13}C$ proxies are consistent with published redox-sensitive trace element records, confirming less-oxygenated deep ocean during the LGP compared to modern. The benthic surface porosity and $\Delta\delta^{13}C$ records suggest glacial BWO ranged from 50 to ~100 μmol/kg in the deep Arabian Sea. The comparison of glacial OMZ profiles between the Arabian Sea and Peruvian Margin suggest slightly better-oxygenated upper ocean and no changes in the OMZ depth boundary in both regions. These emerging semi-quantitative oxygen records during the LGP are valuable targets for future data-model comparison.

Consistent with previous studies, we propose that two mechanisms, one local and one related to high-latitude process, contributed to better oxygenation of the OMZ, overcoming the influence of more oxygen consumption due to higher primary productivity. In the glacial Arabian Sea, colder SST and strong convective mixing (induced by stronger winter monsoon) injected high oxygen surface water into the OMZ. In addition, more AAIW, with higher oxygen concentrations, may have contributed to better oxygenation of the OMZ. The less-oxygenated deep water was likely due to poorly-oxygenated source water originated from the Southern Ocean.

Competing interests

The authors declare no competing interests.

Acknowledgements

We thank WHOI Seafloor Samples Repository and Lamont-Doherty Core Repository for curating and providing the samples, and WHOI NOSAMS for radiocarbon analyses. We thank Steven Clemens (Brown University) for sharing samples of core RC27-61. We thank K. Pietro and B. Monteleone for technical assistance. This work was funded by NSF OCE-1946185 (to K. M.C., D.W.O.), NSF OCE-2114579 (to D.W.O), and WHOI Post-doctoral Scholar Program (to W.L.).

Supplementary Material

All data are publicly available as supporting information to this document.

Table 1. Core summary

Site	Lat	Long	Depth (m)	Modern BWO (µmol/kg)	Proxy (*published)	Age model reference(s)
RC27-14	18.25	57.66	596	6	Surface porosity	Altabet et al., 2002
TN041-8PG/JPC	17.81	57.51	761	7	Surface porosity *	Lu et al., 2022
RC27-23	17.99	57.59	820	7	Surface porosity	Altabet et al., 2002
TN041-2PG	17.70	57.83	1428	42	Surface porosity	This study
GeoB3004	14.60	52.90	1803	82	$\Delta\delta^{13}C$ *	Schmiedl and Mackensen, 2006
RC27-61	16.63	59.86	1890	77	Surface porosity, $\Delta\delta^{13}C$	Clemens and Prell, 1990
RC27-42	16.50	59.80	2020	84	Surface porosity, $\Delta\delta^{13}C$	Pourmand et al., 2007
TN047-6GGC	17.38	58.80	3652	129	Surface porosity, $\Delta\delta^{13}C$	Dahl and Oppo, 2006

Table 2. Radiocarbon dates in core TN041-2PG

LabID	Core	Depth (cm)	Material	^{14}C age (BP yrs)	Age error	Calibrated age (BP yrs)	2 sigma (BP yrs)
OS-170487	TN041-2PG	0.5	*G. ruber*	3290	20	2841	2670 - 3060
OS-170488	TN041-2PG	120.5	*G. ruber*	17850	110	20533	20175 - 20880

Figures and captions

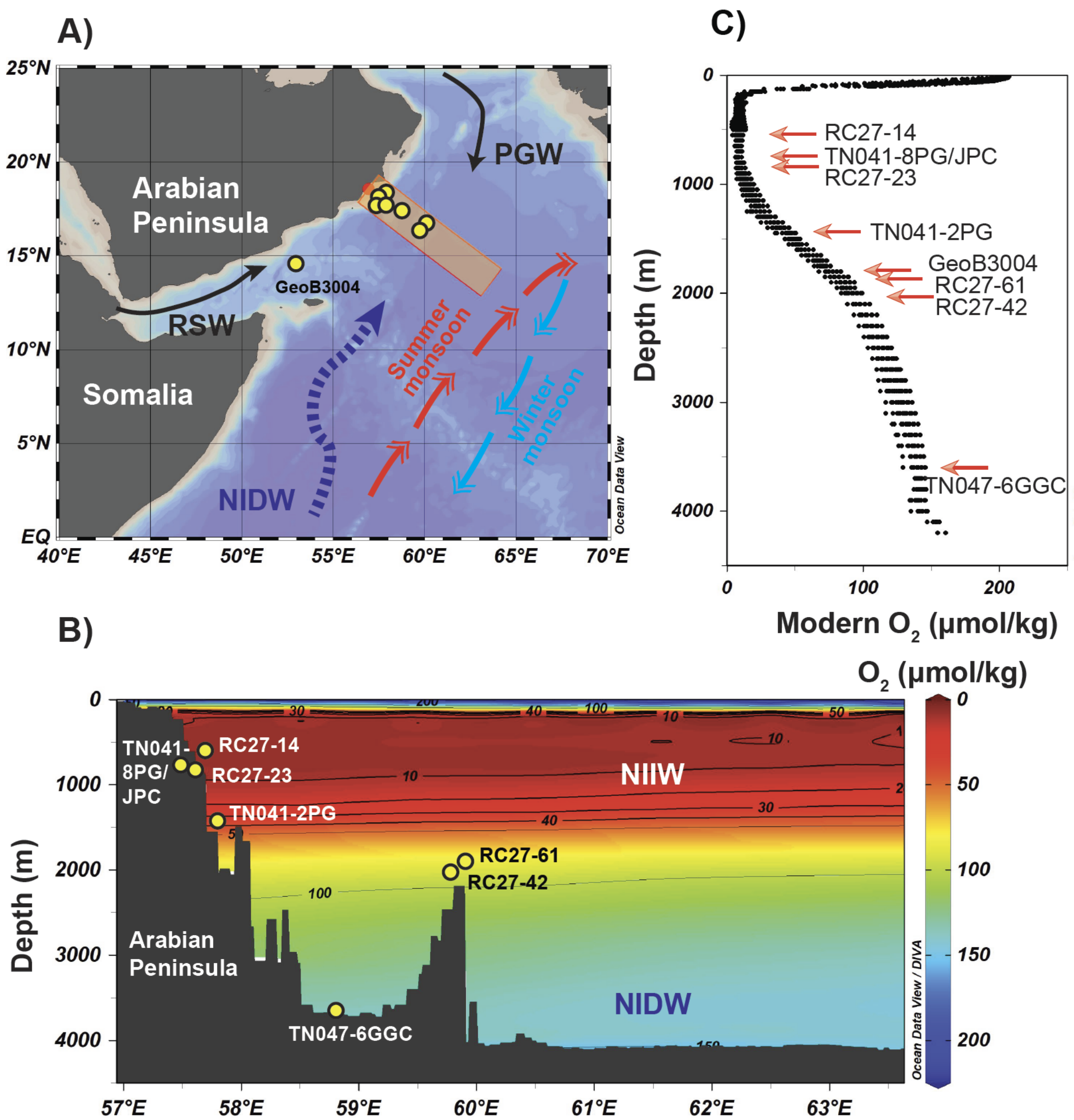

Fig. 1. Sampling locations and dissolved oxygen concentrations in the Arabian Sea. Eight core sites are located within and below the modern OMZ. A) Circulation and water masses in the Arabian Sea. Black solid arrows denote surface water currents, dark blue dash arrow denotes deep water masses, while red and blue arrows denote summer and winter monsoon. RSW: Red Sea Water; PGW: Persian Gulf Water; NIIW: North Indian Intermediate Water; NIDW: North Indian Deep Water. B) Cross section of oxygen concentrations vs. water depth at the study site. The oxygen minimum zone (<20 umol/kg) ranges from 200-1000m. C) Water depth profiles averaged across the Arabian Sea, with core depths superimposed. Figures were generated using Ocean Data View software (Schlitzer, 2021). Oxygen data are from World Ocean Atlas 2018 (Garcia et al., 2019).

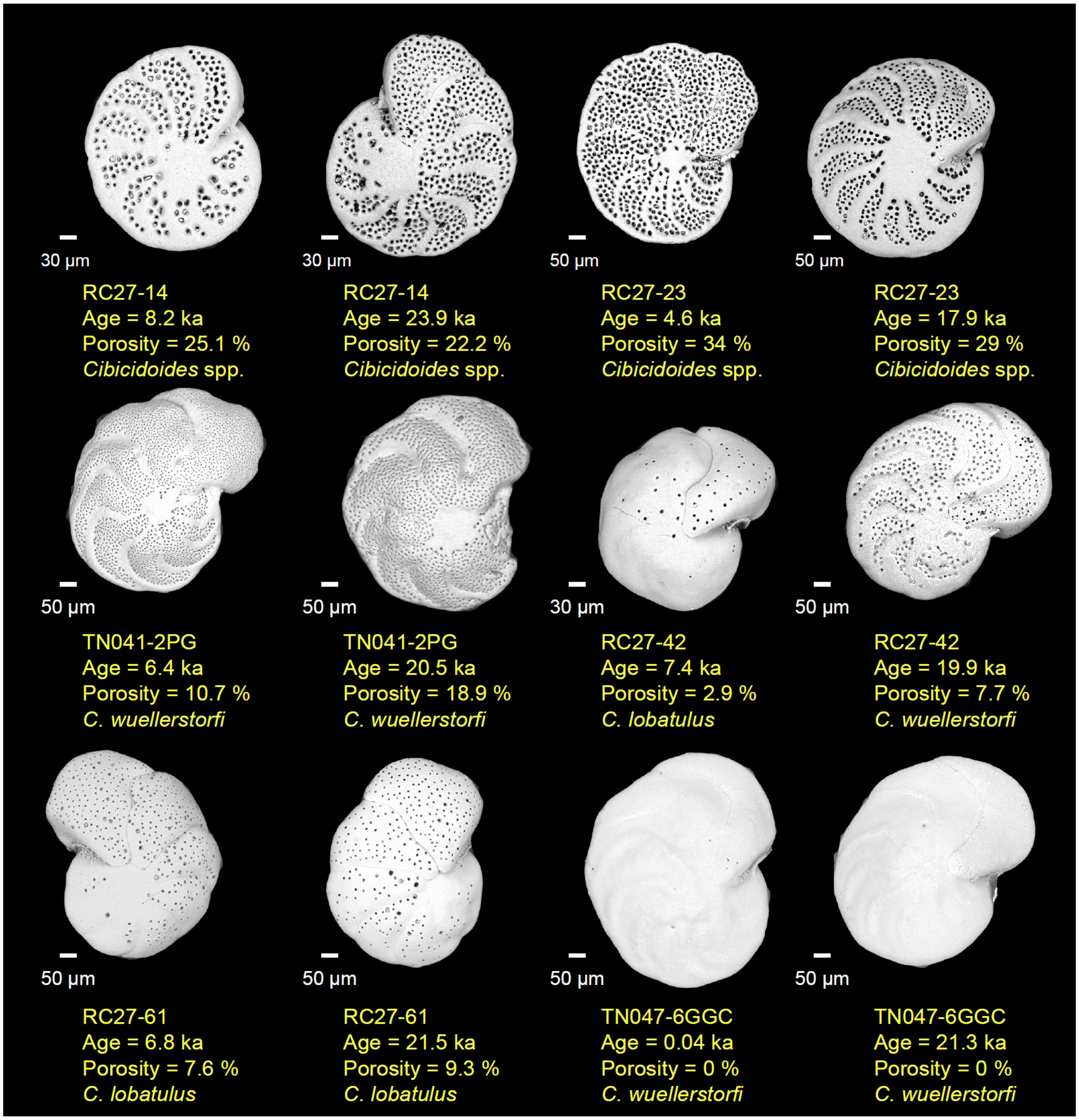

Fig. 2. Representative SEM photos of *Cibicidoides* spp. of Holocene and LGP ages in six cores.

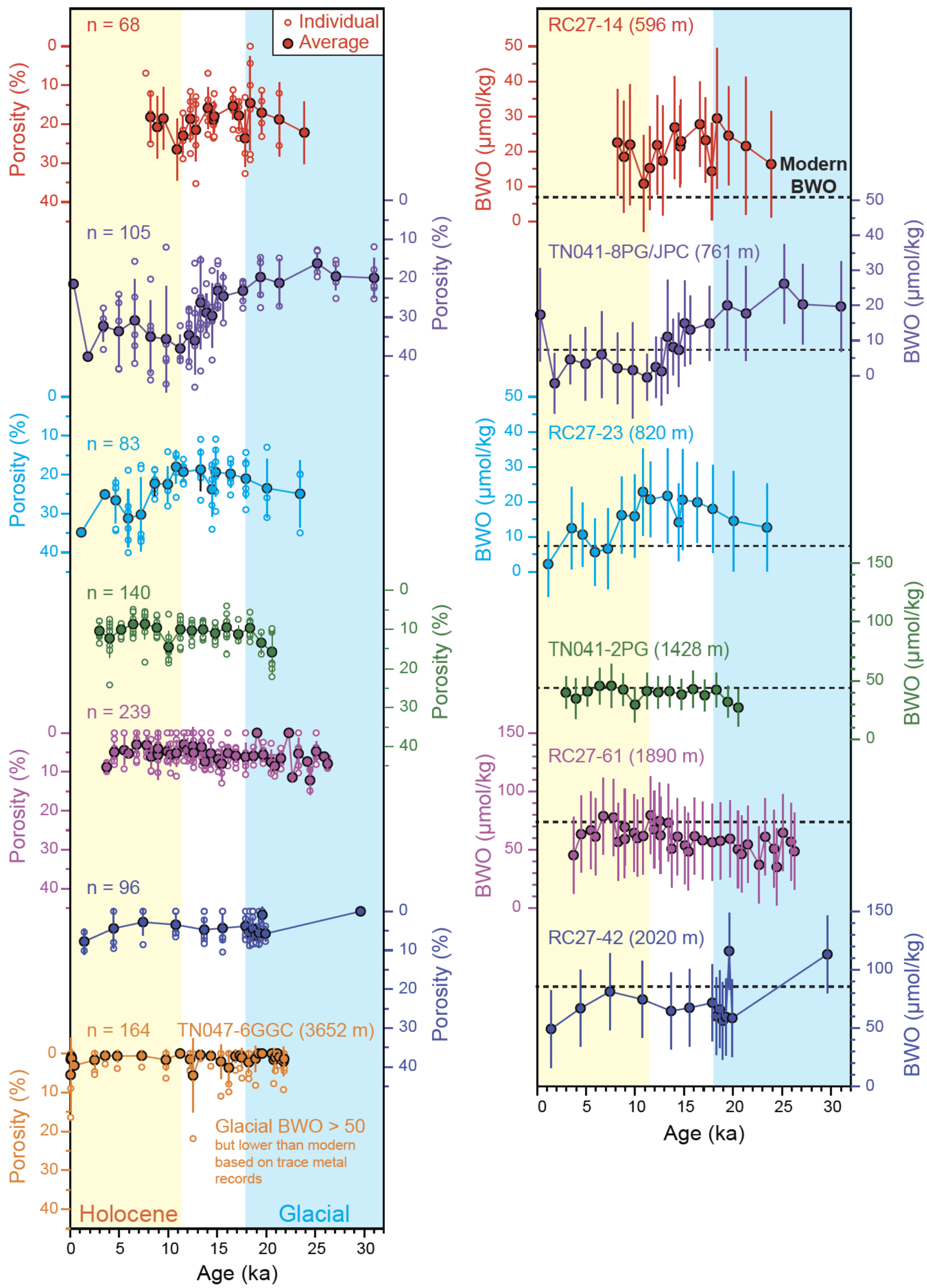

Fig. 3. *Cibicidoides* spp. surface porosity-based BWO records in seven Arabian Sea cores arranged by increasing water depths. The record of TN041-8PG/JPC is from Lu et al. (2022), all other six cores are from this study. In core TN047-6GGC (orange color), persistently low surface porosity (< 10%) indicates that BWO remained above 50 µmol/kg, while other studies using redox-sensitive trace element records have suggest that glacial BWO was still lower than modern value (130 µmol/kg) (Sirocko et al., 2000). Colored bars denote the Holocene (yellow) and last glacial period (blue).

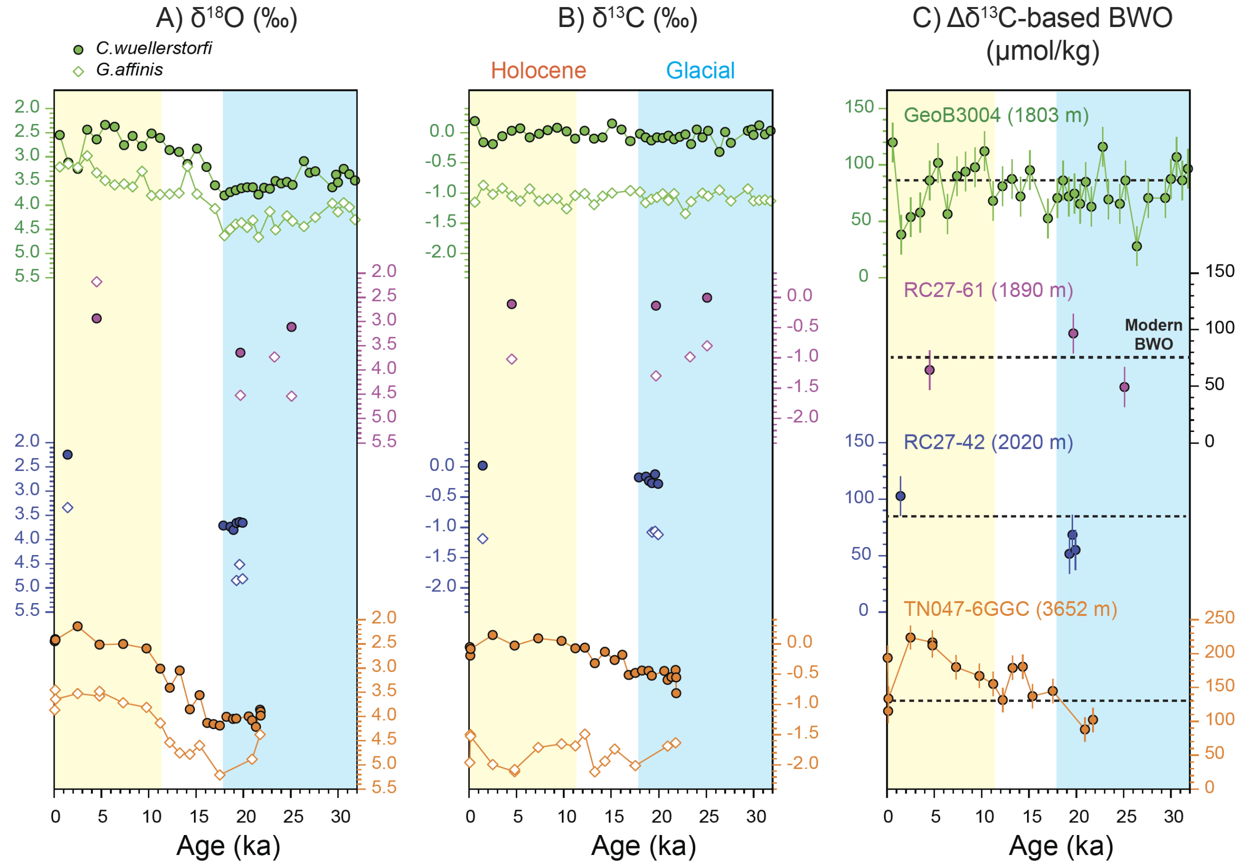

Fig. 4. Benthic isotope records in four core sites and the Δδ^{13}C-based BWO reconstructions. A) δ^{18}O for *C. wuellerstorfi* (solid symbols) and *G. affinis* (open symbols). B) δ^{13}C records for *C. wuellerstorfi* (solid symbols) and *G. affinis* (open symbols). C) Δδ^{13}C-based BWO records. The record of GeoB3004 is from Schmiedl and Mackensen (2006), all other three cores are from this study. The Δδ^{13}C records of two shallower sites suggest similar BWO between modern and LGP, while the two deeper cores suggest lower BWO in LGP relative to modern.

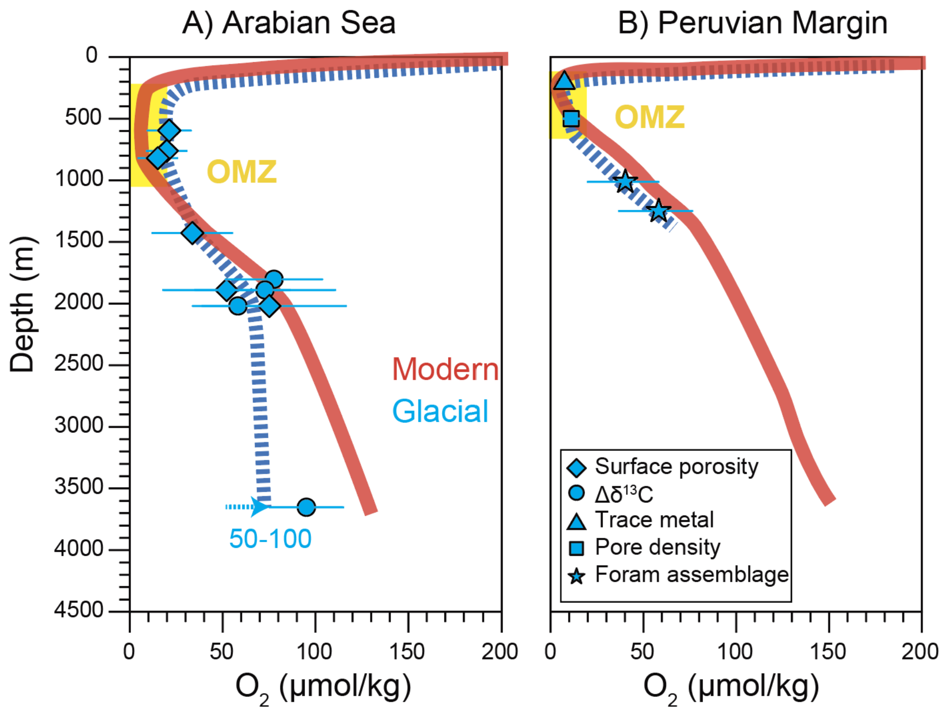

Fig. 5. Modern and glacial oxygen profiles in the Arabian Sea (A) and Peruvian Margin (B). The paleo-BWO records in Peruvian Margin are from Scholz et al. (2014), Erdem et al. (2020), Glock et al. (2022).

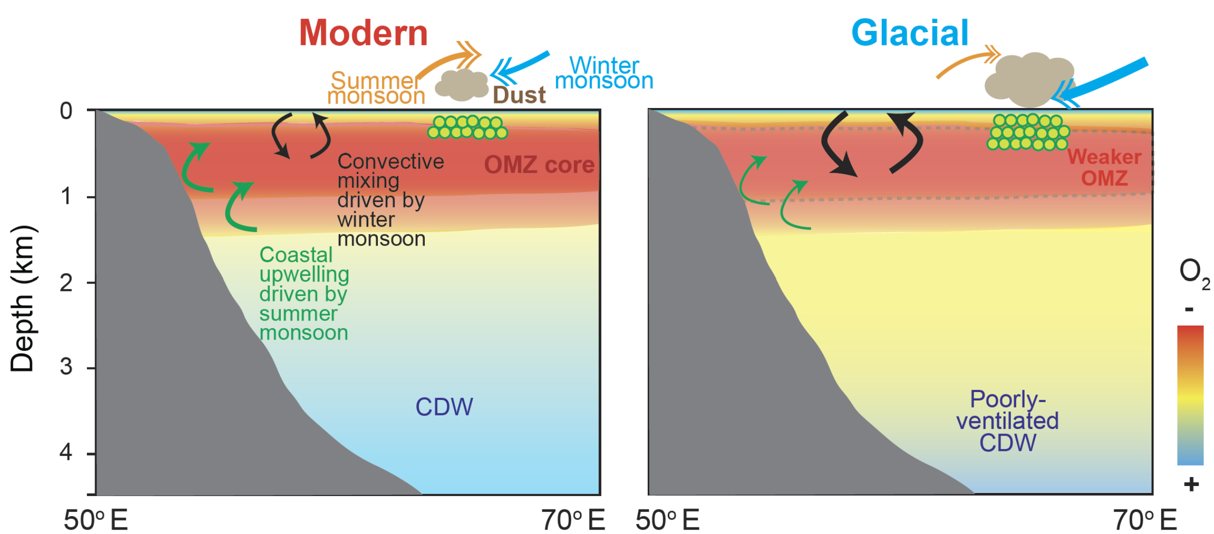

Fig. 6. Potential driving mechanisms of Arabian Sea OMZ in the Modern and Glacial period. The glacial productivity, dust, monsoon, upwelling, convective mixing depths patterns are derived from previously published proxy records (Reichart et al., 1998; Pourmand et al., 2004, 2007; Zhou et al., 2022). Thicker arrows indicate…. The colorbar is qualitative, with blue colors having more oxygen than red colors.

References

Altabet, M. A., Higginson, M. J., & Murray, D. W. (2002). The effect of millennial-scale changes in Arabian Sea denitrification on atmospheric CO2. *Nature*. https://doi.org/10.1038/415159a

Anderson, R. F., Sachs, J. P., Fleisher, M. Q., Allen, K. A., Yu, J., Koutavas, A., & Jaccard, S. L. (2019). Deep-Sea Oxygen Depletion and Ocean Carbon Sequestration During the Last Ice Age. *Global Biogeochemical Cycles*, *33*(3). https://doi.org/10.1029/2018GB006049

Blaauw, M., & Christeny, J. A. (2011). Flexible paleoclimate age-depth models using an autoregressive gamma process. *Bayesian Analysis*, *6*(3). https://doi.org/10.1214/11-BA618

Bopp, L., Resplandy, L., Orr, J. C., Doney, S. C., Dunne, J. P., Gehlen, M., et al. (2013). Multiple stressors of ocean ecosystems in the 21st century: Projections with CMIP5 models. *Biogeosciences*, *10*(10). https://doi.org/10.5194/bg-10-6225-2013

Bopp, L., Resplandy, L., Untersee, A., le Mezo, P., & Kageyama, M. (2017). Ocean (de)oxygenation from the Last Glacial Maximum to the twenty-first century: Insights from Earth System models. *Philosophical Transactions of the Royal Society A: Mathematical, Physical and Engineering Sciences*, *375*(2102). https://doi.org/10.1098/rsta.2016.0323

Breitburg, D., Levin, L. A., Oschlies, A., Grégoire, M., Chavez, F. P., Conley, D. J., et al. (2018). Declining oxygen in the global ocean and coastal waters. *Science*. https://doi.org/10.1126/science.aam7240

Buchanan, P. J., Matear, R. J., Lenton, A., Phipps, S. J., Chase, Z., & Etheridge, D. M. (2016). The simulated climate of the Last Glacial Maximum and insights into the global marine carbon cycle. *Climate of the Past*, *12*(12). https://doi.org/10.5194/cp-12-2271-2016

Clemens, S. C., & Prell, W. L. (1990). Late Pleistocene variability of Arabian Sea summer monsoon winds and continental aridity: Eolian records from the lithogenic component of deep-sea sediments. *Paleoceanography*, *5*(2). https://doi.org/10.1029/PA005i002p00109

Cliff, E., Khatiwala, S., & Schmittner, A. (2021). Glacial deep ocean deoxygenation driven by biologically mediated air–sea disequilibrium. *Nature Geoscience*, *14*(1). https://doi.org/10.1038/s41561-020-00667-z

Costa, K. M., Nielsen, S. G., Wang, Y., Lu, W., Hines, S. K. V., Jacobel, A., & Oppo, D. W. (2023). Marine sedimentary uranium to barium ratios as a potential quantitative proxy for Pleistocene bottom water oxygen concentrations. *Geochimica et Cosmochimica Acta*, *343*, 1–16. https://doi.org/10.1016/j.gca.2022.12.022

Dahl, K. A., & Oppo, D. W. (2006). Sea surface temperature pattern reconstructions in the Arabian Sea. *Paleoceanography*, *21*(1). https://doi.org/10.1029/2005PA001162

Erdem, Z., Schönfeld, J., Rathburn, A. E., Pérez, M. E., Cardich, J., & Glock, N. (2020). Bottom-water deoxygenation at the Peruvian margin during the last deglaciation recorded by benthic foraminifera. *Biogeosciences*, *17*(12). https://doi.org/10.5194/bg-17-3165-2020

Fu, W., Primeau, F., Keith Moore, J., Lindsay, K., & Randerson, J. T. (2018). Reversal of Increasing Tropical Ocean Hypoxia Trends With Sustained Climate Warming. *Global Biogeochemical Cycles*, *32*(4). https://doi.org/10.1002/2017GB005788

Galbraith, E. D., & Jaccard, S. L. (2015). Deglacial weakening of the oceanic soft tissue pump: Global constraints from sedimentary nitrogen isotopes and oxygenation proxies. *Quaternary Science Reviews*, *109*. https://doi.org/10.1016/j.quascirev.2014.11.012

Galbraith, E. D., Kienast, M., Pedersen, T. F., & Calvert, S. E. (2004). Glacial-interglacial modulation of the marine nitrogen cycle by high-latitude O2 supply to the global thermocline. *Paleoceanography*, *19*(4). https://doi.org/10.1029/2003PA001000

Garcia, H. E., Weathers, K., Paver, C. R., Smolyar, I., Boyer, T. P., Locarnini, R. A., et al. (2019). World Ocean Atlas 2018, Volume 3: Dissolved Oxygen, Apparent Oxygen Utilization, and Oxygen Saturation. *NOAA Atlas NESDIS*, *3*(83).

Gaye, B., Böll, A., Segschneider, J., Burdanowitz, N., Emeis, K. C., Ramaswamy, V., et al. (2018). Glacial-interglacial changes and Holocene variations in Arabian Sea denitrification. *Biogeosciences*, *15*(2). https://doi.org/10.5194/bg-15-507-2018
Glock, N., Liebetrau, V., & Eisenhauer, A. (2014). I/Ca ratios in benthic foraminifera from the Peruvian oxygen minimum zone: Analytical methodology and evaluation as a proxy for redox conditions. *Biogeosciences*, *11*(23). https://doi.org/10.5194/bg-11-7077-2014
Glock, N., Erdem, Z., & Schönfeld, J. (2022). The Peruvian oxygen minimum zone was similar in extent but weaker during the Last Glacial Maximum than Late Holocene. *Communications Earth & Environment*, *3*(307).
Glock, N., Erdem, Z., Wallmann, K., Somes, C. J., Liebetrau, V., Schönfeld, J., et al. (2018). Coupling of oceanic carbon and nitrogen facilitates spatially resolved quantitative reconstruction of nitrate inventories. *Nature Communications*, *9*(1). https://doi.org/10.1038/s41467-018-03647-5
Gottschalk, J., Skinner, L. C., Lippold, J., Vogel, H., Frank, N., Jaccard, S. L., & Waelbroeck, C. (2016). Biological and physical controls in the Southern Ocean on past millennial-scale atmospheric CO2 changes. *Nature Communications*, *7*. https://doi.org/10.1038/ncomms11539
Gottschalk, J., Michel, E., Thöle, L. M., Studer, A. S., Hasenfratz, A. P., Schmid, N., et al. (2020). Glacial heterogeneity in Southern Ocean carbon storage abated by fast South Indian deglacial carbon release. *Nature Communications*, *11*(1). https://doi.org/10.1038/s41467-020-20034-1
Heaton, T. J., Köhler, P., Butzin, M., Bard, E., Reimer, R. W., Austin, W. E. N., et al. (2020). Marine20 - The Marine Radiocarbon Age Calibration Curve (0-55,000 cal BP). *Radiocarbon*, *62*(4). https://doi.org/10.1017/RDC.2020.68
Hoogakker, B. A. A., Elderfield, H., Schmiedl, G., McCave, I. N., & Rickaby, R. E. M. (2015). Glacial-interglacial changes in bottom-water oxygen content on the Portuguese margin. *Nature Geoscience*, *8*(1). https://doi.org/10.1038/ngeo2317
Hoogakker, B. A. A., Lu, Z., Umling, N., Jones, L., Zhou, X., Rickaby, R. E. M., et al. (2018). Glacial expansion of oxygen-depleted seawater in the eastern tropical Pacific. *Nature*, *562*(7727). https://doi.org/10.1038/s41586-018-0589-x
Jaccard, S. L., & Galbraith, E. D. (2012). Large climate-driven changes of oceanic oxygen concentrations during the last deglaciation. *Nature Geoscience*, *5*(2). https://doi.org/10.1038/ngeo1352
Jacobel, A. W., Anderson, R. F., Jaccard, S. L., McManus, J. F., Pavia, F. J., & Winckler, G. (2020). Deep Pacific storage of respired carbon during the last ice age: Perspectives from bottom water oxygen reconstructions. *Quaternary Science Reviews*. https://doi.org/10.1016/j.quascirev.2019.106065
Keeling, R. F., Körtzinger, A., & Gruber, N. (2010). Ocean deoxygenation in a warming world. *Annual Review of Marine Science*, *2*(1). https://doi.org/10.1146/annurev.marine.010908.163855
Lachkar, Z., Lévy, M., & Smith, K. S. (2019). Strong Intensification of the Arabian Sea Oxygen Minimum Zone in Response to Arabian Gulf Warming. *Geophysical Research Letters*, *46*(10). https://doi.org/10.1029/2018GL081631
Lachkar, Zouhair, Lévy, M., & Smith, S. (2018). Intensification and deepening of the Arabian Sea oxygen minimum zone in response to increase in Indian monsoon wind intensity. *Biogeosciences*, *15*(1). https://doi.org/10.5194/bg-15-159-2018
Lathika, N., Rahaman, W., Tarique, M., Gandhi, N., Kumar, A., & Thamban, M. (2021). Deep water circulation in the Arabian Sea during the last glacial cycle: Implications for paleo-redox condition, carbon sink and atmospheric CO2 variability. *Quaternary Science Reviews*, *257*. https://doi.org/10.1016/j.quascirev.2021.106853
Lu, W., Rickaby, R. E. M., Hoogakker, B. A. A., Rathburn, A. E., Burkett, A. M., Dickson, A. J., et al. (2020). I/Ca in epifaunal benthic foraminifera: A semi-quantitative proxy for bottom water oxygen in a multi-proxy compilation for glacial ocean deoxygenation. *Earth and Planetary Science Letters*, *533*. https://doi.org/10.1016/j.epsl.2019.116055

Lu, W., Wang, Y., Oppo, D. W., Nielsen, S. G., & Costa, K. M. (2022). Comparing paleo-oxygenation proxies (benthic foraminiferal surface porosity, I/Ca, authigenic uranium) on modern sediments and the glacial Arabian Sea. *Geochimica et Cosmochimica Acta*. https://doi.org/10.1016/J.GCA.2022.06.001

McCorkle, D. C., & Emerson, S. R. (1988). The relationship between pore water carbon isotopic composition and bottom water oxygen concentration. *Geochimica et Cosmochimica Acta*, *52*(5). https://doi.org/10.1016/0016-7037(88)90270-0

Meissner, K. J., Galbraith, E. D., & Völker, C. (2005). Denitrification under glacial and interglacial conditions: A physical approach. *Paleoceanography*, *20*(3). https://doi.org/10.1029/2004PA001083

Moffitt, S. E., Moffitt, R. A., Sauthoff, W., Davis, C. v., Hewett, K., & Hill, T. M. (2015). Paleoceanographic insights on recent oxygen minimum zone expansion: Lessons for modern oceanography. *PLoS ONE*. https://doi.org/10.1371/journal.pone.0115246

Morrison, J. M., Codispoti, L. A., Smith, S. L., Wishner, K., Flagg, C., Gardner, W. D., et al. (1999). The oxygen minimum zone in the Arabian Sea during 1995. *Deep-Sea Research Part II: Topical Studies in Oceanography*, *46*(8–9). https://doi.org/10.1016/S0967-0645(99)00048-X

Muratli, J. M., Chase, Z., Mix, A. C., & McManus, J. (2010). Increased glacial-age ventilation of the Chilean margin by Antarctic Intermediate Water. *Nature Geoscience*, *3*(1). https://doi.org/10.1038/ngeo715

Nair, R. R., Ittekkot, V., Manganini, S. J., Ramaswamy, V., Haake, B., Degens, E. T., et al. (1989). Increased particle flux to the deep ocean related to monsoons. *Nature*, *338*(6218). https://doi.org/10.1038/338749a0

Naqvi, S. W. A. (1987). Some aspects of the oxygen-deficient conditions and denitrification in the Arabian Sea. *Journal of Marine Research*, *45*(4). https://doi.org/10.1357/002224087788327118

Olson, D. B., Hitchcock, G. L., Fine, R. A., & Warren, B. A. (1993). Maintenance of the low-oxygen layer in the central Arabian Sea. *Deep-Sea Research Part II*, *40*(3). https://doi.org/10.1016/0967-0645(93)90051-N

Petersen, J., Riedel, B., Barras, C., Pays, O., Guihéneuf, A., Mabilleau, G., et al. (2016). Improved methodology for measuring pore patterns in the benthic foraminiferal genus Ammonia. *Marine Micropaleontology*, *128*. https://doi.org/10.1016/j.marmicro.2016.08.001

Pichevin, L., Bard, E., Martinez, P., & Billy, I. (2007). Evidence of ventilation changes in the Arabian Sea during the late Quaternary: Implication for denitrification and nitrous oxide emission. *Global Biogeochemical Cycles*, *21*(4). https://doi.org/10.1029/2006GB002852

Piotrowski, A. M., Banakar, V. K., Scrivner, A. E., Elderfield, H., Galy, A., & Dennis, A. (2009). Indian Ocean circulation and productivity during the last glacial cycle. *Earth and Planetary Science Letters*, *285*(1–2). https://doi.org/10.1016/j.epsl.2009.06.007

Pourmand, A., Marcantonio, F., Bianchi, T. S., Canuel, E. A., & Waterson, E. J. (2007). A 28-ka history of sea surface tempeture, primary productivity and planktonic community variability in the western Arabian Sea. *Paleoceanography*, *22*(4). https://doi.org/10.1029/2007PA001502

Rathburn, A. E., Willingham, J., Ziebis, W., Burkett, A. M., & Corliss, B. H. (2018). A New biological proxy for deep-sea paleo-oxygen: Pores of epifaunal benthic foraminifera. *Scientific Reports*, *8*(1). https://doi.org/10.1038/s41598-018-27793-4

Reichart, G. J., Lourens, L. J., & Zachariasse, W. J. (1998). Temporal variability in the northern Arabian Sea oxygen minimum zone (OMZ) during the last 225,000 years. *Paleoceanography*, *13*(6). https://doi.org/10.1029/98PA02203

Resplandy, L. (2018). Will ocean zones with low oxygen levels expand or shrink? news-and-views. *Nature*, *557*(7705). https://doi.org/10.1038/d41586-018-05034-y

Rohling, E. J., & Zachariasse, W. J. (1996). Red Sea outflow during the last glacial maximum. *Quaternary International*, *31*. https://doi.org/10.1016/1040-6182(95)00023-C

Schlitzer, R. (2021). Ocean Data View. Retrieved from https://odv.awi.de/
Schmidtko, S., Stramma, L., & Visbeck, M. (2017). Decline in global oceanic oxygen content during the past five decades. *Nature*, *542*(7641). https://doi.org/10.1038/nature21399
Schmiedl, G., & Leuschner, D. C. (2005). Oxygenation changes in the deep western Arabian Sea during the last 190,000 years: Productivity versus deepwater circulation. *Paleoceanography*, *20*(2). https://doi.org/10.1029/2004PA001044
Schmiedl, G., & Mackensen, A. (2006). Multispecies stable isotopes of benthic foraminifers reveal past changes of organic matter decomposition and deepwater oxygenation in the Arabian Sea. *Paleoceanography*, *21*(4). https://doi.org/10.1029/2006PA001284
Schmittner, A., & Somes, C. J. (2016). Complementary constraints from carbon (13C) and nitrogen (15N) isotopes on the glacial ocean's soft-tissue biological pump. *Paleoceanography*, *31*(6). https://doi.org/10.1002/2015PA002905
Scholz, F., Mcmanus, J., Mix, A. C., Hensen, C., & Schneider, R. R. (2014). The impact of ocean deoxygenation on iron release from continental margin sediments. *Nature Geoscience*, *7*(6). https://doi.org/10.1038/ngeo2162
Schulte, S., Rostek, F., Bard, E., Rullkötter, J., & Marchal, O. (1999). Variations of oxygen-minimum and primary productivity recorded in sediments of the Arabian Sea. *Earth and Planetary Science Letters*, *173*(3). https://doi.org/10.1016/S0012-821X(99)00232-0
Sirocko, F., Sirocko, F., Devey, C., & Garbe-Schönberg, D. (2000). Processes controlling trace element geochemistry of Arabian Sea sediments during the last 25,000 years. *Global and Planetary Change*, *26*(1–3). https://doi.org/10.1016/S0921-8181(00)00046-1
Somes, C. J., Schmittner, A., Muglia, J., & Oschlies, A. (2017). A three-dimensional model of the marine nitrogen cycle during the last glacial maximum constrained by sedimentary isotopes. *Frontiers in Marine Science*, *4*(MAY). https://doi.org/10.3389/fmars.2017.00108
Stuiver, M., Reimer, P., & Reimer, R. (2022). CALIB 8.2.
Tetard, M., Licari, L., Ovsepyan, E., Tachikawa, K., & Beaufort, L. (2021). Toward a global calibration for quantifying past oxygenation in oxygen minimum zones using benthic Foraminifera. *Biogeosciences*, *18*(9). https://doi.org/10.5194/bg-18-2827-2021
Yamamoto, A., Abe-Ouchi, A., Ohgaito, R., Ito, A., & Oka, A. (2019). Glacial CO2 decrease and deep-water deoxygenation by iron fertilization from glaciogenic dust. *Climate of the Past*, *15*(3). https://doi.org/10.5194/cp-15-981-2019
You, Y. (2000). Implications of the deep circulation and ventilation of the Indian Ocean on the renewal mechanism of North Atlantic Deep Water. *Journal of Geophysical Research: Oceans*, *105*(C10). https://doi.org/10.1029/2000jc900105
Yu, Z., Colin, C., Ma, R., Meynadier, L., Wan, S., Wu, Q., et al. (2018). Antarctic Intermediate Water penetration into the Northern Indian Ocean during the last deglaciation. *Earth and Planetary Science Letters*, *500*. https://doi.org/10.1016/j.epsl.2018.08.006
Zhou, Y., Duchamp-Alphonse, S., Kageyama, M., Bassinot, F., Doressoundiram, F., & Kissel, C. (2022). Variations of Primary Productivity in the Northwestern Arabian Sea During the Last 23,000 Years and Their Paleoclimatological Implications. *Paleoceanography and Paleoclimatology*, *37*, e2022PA004453. https://doi.org/10.1029/2022PA004453